phase can be observed, which accommodate the imposed boundary condition in a reversible way (this is the origin of the memory effect). □

Methods

To prove that in a reconstructive transformation an aperiodic element of $\mathcal{G}$ (called GL(3, $\mathbb{Z}$) in algebra) is generated, we first note that any lattice group is finite, and conversely any finite subgroup of $\mathcal{G}$ is included in the lattice group of some lattice (see proposition 3.5 in ref. 23). Thus a transformation is weak if and only if the lattice groups of the two crystal phases generate a finite group. Therefore a reconstructive transformation produces an infinite subgroup of $\mathcal{G}$ with a finite number of generators. Such a group necessarily contains an element with no finite period as a consequence of the Burnside–Schur theorem on periodic groups.

We finally establish that for any pair of Bravais lattices with maximal point symmetry there are reconstructive transformations that generate the entire group $\mathcal{G}$. Indeed, it is readily verified that for suitable pairs of subgroups in $\mathcal{G}$ belonging to the four arithmetic classes with maximal point symmetry one can produce all the generators of $\mathcal{G}$, that is, a suitable reflection, permutation and simple shear[30].

Received 2 September 2003; accepted 28 January 2004; doi:10.1038/nature02378.

1. Olson, G. B. & Owen, W. (eds) *Martensite* (ASM International, Materials Park, OH, 1992).
2. Salje, E. K. H. *Phase Transitions in Ferroelastic and Co-elastic Crystals* (Cambridge Univ. Press, Cambridge, 1993).
3. Otsuka, K. & Wayman, C. M. *Shape Memory Materials* (Cambridge Univ. Press, Cambridge, 1998).
4. Barrett, C. S. & Massalski, T. B. *Structure of Metals* 3rd edn (Pergamon, Oxford, 1987).
5. Bocanegra-Bernal, M. H. & De la Torre, S. D. Phase transitions in zirconium dioxide and related materials for high performance engineering ceramics. *J. Mater. Sci.* **37,** 4947–4971 (2002).
6. Olson, G. B. & Hartman, H. Martensite and life—displacive transformations as biological processes. *J. Physique* **43**(C4), 855–865 (1982).
7. James, R. D. & Wuttig, M. Magnetostriction of martensite. *Phil. Mag. A* **77,** 1273–1299 (1998).
8. Sozinov, A., Likhachev, A. A., Lanska, N. & Ullakko, K. Giant magnetic-field-induced strain in NiMnGa seven-layered martensitic phase. *Appl. Phys. Lett.* **80,** 1746–1748 (2002).
9. Shu, Y. C. & Bhattacharya, K. Domain patterns and macroscopic behaviour of ferroelectric materials. *Phil. Mag. B* **81,** 2021–2054 (2001).
10. de Gennes, P.-G. & Okumura, K. Phase transitions of nematic rubbers. *Europhys. Lett.* **63,** 76–82 (2003).
11. Bhattacharya, K. *Microstructure of Martensite: Why it Forms and How it Gives Rise to the Shape-Memory Effect* (Oxford Univ. Press, Oxford, 2003).
12. Ericksen, J. L. Weak martensitic transformations in Bravais lattices. *Arch. Ration. Mech. Anal.* **107,** 23–36 (1989).
13. Tolédano, P. & Dmitriev, V. *Reconstructive Phase Transitions* (World Scientific, Singapore, 1996).
14. Maki, T. & Tamura, I. in *Proc. Int. Conf. on Martensitic Transformations* 963–970 (The Japan Institute of Metals, Nara, 1986).
15. Barker, L. M. & Hollenbach, R. E. Shock wave study of the $\alpha \leftrightarrow \varepsilon$ phase transition in iron. *J. Appl. Phys.* **45,** 4872–4887 (1974).
16. Kadau, K., Germann, T. C., Lomdahl, P. S. & Holian, B. L. Microscopic view of structural phase transitions induced by shock waves. *Science* **296,** 1681–1684 (2002).
17. Liu, Y. *et al.* Thermomechanical behaviour of fcc ↔ hcp martensitic transformation in CoNi. *J. Alloys Compd.* (in the press).
18. Matsumoto, S., Sato, A. & Mori, T. Formation of h.c.p. and f.c.c. twins in an Fe-Mn-Cr-Si-Ni alloy. *Acta Metall. Mater.* **42,** 1207–1213 (1994).
19. Yang, J. H. & Wayman, C. M. On secondary variants formed at intersections of ε martensite variants. *Acta Metall. Mater.* **40,** 2011–2023 (1992).
20. Lee, H. H. *et al.* Orientational proliferation and successive twinning from thermoreversible hexagonal-body-centered cubic transitions. *Macromolecules* **35,** 785–794 (2002).
21. Otsuka, K. & Shimizu, K. On the crystallographic reversibility of martensitic transformations. *Scripta Met.* **11,** 757–760 (1977).
22. Schwarzenberger, R. L. E. Classification of crystal lattices. *Proc. Camb. Phil. Soc.* **72,** 325–349 (1972).
23. Pitteri, M. & Zanzotto, G. *Continuum Models for Phase Transitions and Twinning in Crystals* (Chapman & Hall/CRC, Boca Raton, 2002).
24. Ericksen, J. L. Some phase transitions in crystals. *Arch. Ration. Mech. Anal.* **73,** 99–124 (1980).
25. Pitteri, M. Reconciliation of local and global symmetries of crystals. *J. Elast.* **14,** 175–190 (1984).
26. Ball, J. M. & James, R. D. Proposed experimental tests of a theory of fine microstructure and the two-well problem. *Phil. Trans. R. Soc. Lond. A* **338,** 389–450 (1992).
27. Fonseca, I. Variational methods for elastic crystals. *Arch. Ration. Mech. Anal.* **97,** 189–220 (1987).
28. Hull, D. & Bacon, D. J. *Introduction to Dislocations* 3rd edn (Pergamon, Oxford, 1984).
29. Conti, S. & Zanzotto, G. A variational model for reconstructive phase transformations in crystals, and their relation to dislocations and plasticity. *Arch. Ration. Mech. Anal.* (in the press).
30. Hua, L. K. & Reiner, I. On the generators of the symplectic modular group. *Trans. Am. Math. Soc.* **65,** 415–426 (1949).

Acknowledgements This work was largely carried out when J.Z. held a position at the California Institute of Technology. The work of S.C. and J.Z. was partially supported by the Deutsche Forschungsgemeinschaft. G.Z. acknowledges the partial support of the Italian MIUR (CoFin Modelli Matematici per i Materiali). S.C. and G.Z. acknowledge the partial support of the IV Framework Programme of the EU. K.B. and J.Z. acknowledge the partial financial support of the US Air Force Office of Scientific Research and the US Office of Naval Research. All authors contributed equally to this work.

Competing interests statement The authors declare that they have no competing financial interests.

Correspondence and requests for materials should be addressed to K.B. (bhatta@caltech.edu).

Polar ocean stratification in a cold climate

Daniel M. Sigman[1], Samuel L. Jaccard[2] & Gerald H. Haug[3]

[1]*Department of Geosciences, Princeton University, Princeton, New Jersey 08544, USA*
[2]*Department of Earth Sciences, ETH, CH-8092 Zürich, Switzerland*
[3]*Geoforschungszentrum Potsdam, D-14473 Potsdam, Germany*

The low-latitude ocean is strongly stratified by the warmth of its surface water. As a result, the great volume of the deep ocean has easiest access to the atmosphere through the polar surface ocean. In the modern polar ocean during the winter, the vertical distribution of temperature promotes overturning, with colder water over warmer, while the salinity distribution typically promotes stratification, with fresher water over saltier. However, the sensitivity of seawater density to temperature is reduced as temperature approaches the freezing point, with potential consequences for global ocean circulation under cold climates[1,2]. Here we present deep-sea records of biogenic opal accumulation and sedimentary nitrogen isotopic composition from the Subarctic North Pacific Ocean and the Southern Ocean. These records indicate that vertical stratification increased in both northern and southern high latitudes 2.7 million years ago, when Northern Hemisphere glaciation intensified in association with global cooling during the late Pliocene epoch. We propose that the cooling caused this increased stratification by weakening the role of temperature in polar ocean density structure so as to reduce its opposition to the stratifying effect of the vertical salinity distribution. The shift towards stratification in the polar ocean 2.7 million years ago may have increased the quantity of carbon dioxide trapped in the abyss, amplifying the global cooling.

The Subarctic Zone in the North Pacific Ocean and the Antarctic Zone in the Southern Ocean are both characterized by year-round availability of the 'major nutrients' nitrate and phosphate. Nutrient-rich deep water is brought to the surface by wind-driven upwelling and density-driven overturning. Limitation of algal growth by light[3] and iron[4] prevents complete consumption of the major nutrients. The Subarctic Pacific maintains a higher degree of nutrient utilization (and thus lower surface nutrient concentrations) than does the Antarctic[5]. There are two likely causes for this difference. First, the exchange between the surface and deep ocean is reduced in the Subarctic Pacific relative to the Antarctic. This is partially due to the stronger 'halocline', or vertical salinity gradient, in the Subarctic Pacific[6] (Fig. 1). Second, atmospheric deposition supplies more iron to the Subarctic Pacific than to the Antarctic, which should allow phytoplankton to consume a larger fraction of the upwelled nitrate and phosphate[4].

Despite the differences between these two polar ocean regions, the sediments underlying them show a similar change during the global cooling from the relatively warm mid-Pliocene to the late Pliocene, when the Earth descended into the Pleistocene cycle of ice ages. In both of these regions, upon the intensification of major Northern Hemisphere glaciation 2.7 million years ago (2.7 Myr), the accumulation of biogenic opal decreased abruptly, just when the sedimentary evidence indicates an increase in Northern Hemisphere sea ice and icebergs[7,8] (Figs 1 and 2; additional references in Fig. 1 legend). In the Antarctic, this shift has been interpreted as the result of increased sea ice cover shortening the productive season of diatoms[8,9], whereas the Subarctic Pacific change has been explained as the onset of permanent stratification reducing the nutrient supply to the surface[7]. Yet the similarity in the structure and timing of these changes invites a single explanation

that would apply in both hemispheres. To distinguish between the very different alternative explanations that have been posed for the 2.7-Myr decrease in opal accumulation, we have measured the $^{15}N/^{14}N$ ratio of bulk sediments as an indicator of nitrate utilization (see Methods). Oceanic phytoplankton preferentially consume ^{14}N-nitrate over ^{15}N-nitrate, resulting in lower sediment $^{15}N/^{14}N$ under more nitrate-replete conditions (that is, the more the gross physical supply of nitrate exceeds the biological assimilation of nitrate)[10].

In the Subarctic Pacific record, sediment $^{15}N/^{14}N$ increases markedly at the 2.7-Myr event, simultaneously with the decrease in opal accumulation (Fig. 2a, inset) and the increase in ice-rafted debris[7], suggesting more complete consumption of surface nitrate subsequent to the intensification of Northern Hemisphere glaciation. This result is consistent with the observation that diatom opal export in the modern Subarctic Pacific could not increase by more than 30% before silicate would be completely absent from the summertime surface layer[11], which indicates that the sharp drop in opal flux at 2.7 Myr cannot be attributed to a decrease in the completeness of silicate consumption. Together, the records of $^{15}N/^{14}N$ and opal accumulation rate make a strong case that the sedimentary change at 2.7 Myr records a decrease in the rate of exposure of nutrient-bearing deep water at the Subarctic Pacific surface. After the 2.7-Myr event, cycles appear, with lower opal flux and higher $^{15}N/^{14}N$ found at intervals that represent the cold phases/ice volume maxima associated with the 41-kyr (obliquity) component of the Milankovitch cycles (Fig. 2a, inset), suggestive of continued climate-induced oscillations in stratification[12].

In the Antarctic record from Ocean Drilling Program (ODP) Site 1096, over the sediment interval recording the change in opal flux to the sea floor, there is no significant change in the sediment $^{15}N/^{14}N$ (Fig. 2b). If the threefold decrease in diatom export suggested by the opal accumulation change were driven by a decrease in the degree of nitrate consumption, the $^{15}N/^{14}N$ of sinking organic matter should have been roughly 3‰ higher before the 2.7-Myr shift[13]. As in the Subarctic Pacific, this suggests that the decrease in opal accumulation rate was not driven by a decrease in the degree to which nutrients were consumed in the surface layer. Rather, the data suggest that the supply of nutrients decreased. While silicate consumption is far from complete in parts of the Antarctic, essentially all of the silicate is consumed within ~5° latitude of the Polar Front in the regions where it has been studied[14], and the 2.7-Myr decrease in opal accumulation observed at ODP Site 1096 has been noted from various sites in the Antarctic (black dots in Fig. 1, references in legend), several of which are close to the Polar Front (the dashed line in Fig. 1) and most of which are overlain by surface waters that are silicate-poor by the end of the summer[5]. Therefore, the modern surface distribution of dissolved silicate suggests strongly that the decrease in opal accumulation at 2.7 Myr was not solely due to a decrease in the opal:carbon ratio of export production[15], as this change alone would require that, after 2.7 Myr, surface waters became extremely enriched in silicate. Although the modern ocean may not be an ideal reflection of mean post-2.7 Myr conditions, interglacials similar to the current one should be reflected in the post-2.7 Myr interval of the sediment records in Fig. 1. Thus, as in the Subarctic Pacific, the $^{15}N/^{14}N$ and opal data together indicate that the nutrient supply to the surface was much greater before the late Pliocene cooling event, suggestive of a subsequent shift towards stratification.

That the apparent degree of nitrate utilization increased at 2.7 Myr in the Subarctic Pacific but remained constant in the Antarctic is consistent with the iron budget in these different regions. In the Subarctic Pacific, where a significant fraction of the iron supply comes from the atmosphere[4], algal productivity

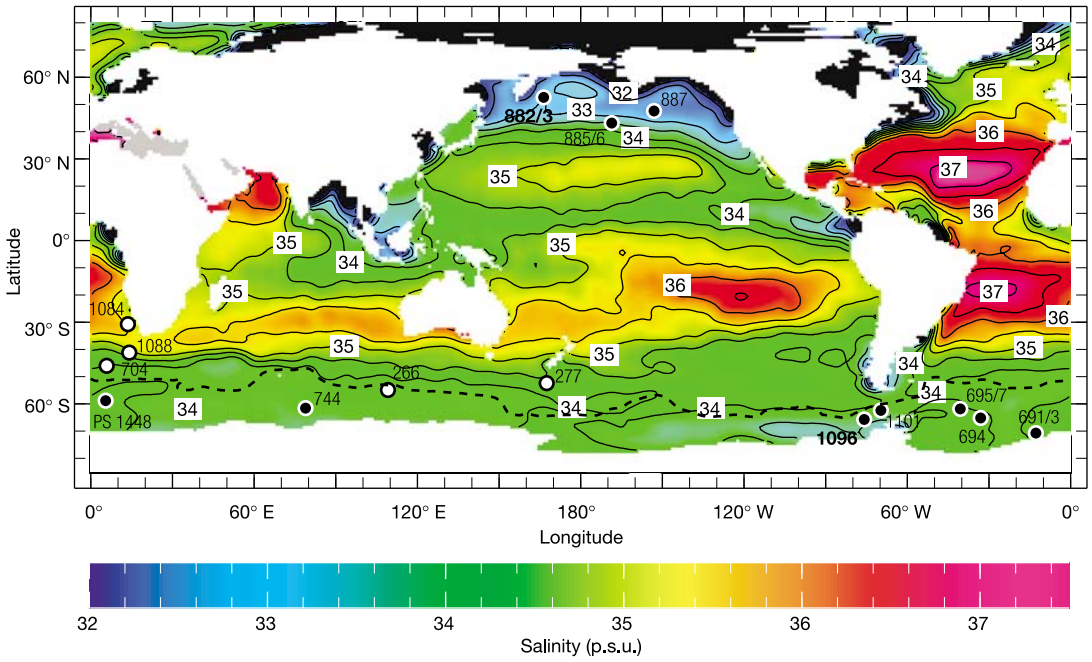

Figure 1 Map of mean annual surface salinity[5] illustrating the predominance of low-salinity surface waters at high latitudes, including the Subarctic North Pacific and the Antarctic. The Antarctic Polar Front, the northern boundary of the Antarctic, is indicated by the dashed line in the Southern Ocean[26]. Filled circles indicate ODP sites where biogenic opal accumulation decreased during the late Pliocene (the sediment cores shown in Fig. 2 are in bold), whereas open circles show locations where opal accumulation increased during roughly the same time interval[7–9,25,27–30]. The broad distribution of the opal decrease within both the Subarctic North Pacific and the Antarctic argues against lateral sediment transport as the cause of the opal accumulation decrease. The increase in opal accumulation at lower latitudes may have been driven by an increase in the oceanic silicate concentration resulting from the drop in opal burial in the polar regions.

would not be strictly limited by the amount of dissolved iron imported from deep water, so that the degree of nitrate consumption should increase in response to stratification. In contrast, in the Antarctic, where nearly all of the iron supply is from upwelled deep water, productivity should decrease as deep water supply decreases, so that the fraction of the nitrate supply that is consumed should remain constant in the face of stratification[16]. Moreover, the lack of any evidence for iron enrichment in the Antarctic provides an additional argument against a decrease in the opal:carbon ratio of export production at the 2.7-Myr transition.

These data fit into a growing body of evidence for a pervasive link between cold climates and polar ocean stratification during the late Cenozoic. Stronger stratification has been proposed for the Antarctic surface during late Pleistocene glacial periods[17,18] and for the last glacial Okhotsk Sea and western Subarctic North Pacific[12]. The well-studied reduction in deep water formation in the high-latitude North Atlantic during ice ages[19] is, in essence, a shift towards stratification in that region. While efforts to explain the stratification of the glacial North Atlantic have focused on changing freshwater inputs[20], the strong correlation of reduced deep water formation with cold periods is most suggestive of cooling as the direct cause of stratification.

The vertical stability of the polar ocean is controlled by the typically opposing effects of temperature (destabilizing) and salinity (stabilizing) (Fig. 3a), but density is less dependent on temperature at lower temperatures. As a result, as the mean temperature of the ocean decreases, a given temperature difference between the surface and deep water would cause a smaller density difference. Thus, homogeneous cooling of the polar ocean water column would cause the vertical temperature gradient to be less important in setting the density gradient, rendering the existing salinity gradient more capable of maintaining year-round polar ocean stratification. Models have shown that stratification of the North Atlantic during glacial times could be the result of global ocean cooling, given the nonlinear sensitivity of seawater density to temperature[1,21].

The importance of global ocean temperature to stratification in other polar regions can be illustrated by recalculating the density profile of the wintertime Antarctic under conditions of higher and lower temperature than today (Fig. 3). If the entire water column is warmed by 3 °C, the modern surface-to-subsurface density difference is removed, such that there would be no barrier to overturning (Fig. 3b, red crosses compared to bold black 'plus' symbols). On the other hand, cooling the entire water column by 2 °C causes an approximate doubling of the modern surface-to-subsurface density difference (Fig. 3c, blue crosses compared to bold black 'plus' symbols). Such a cooling is actually impossible, as the wintertime surface is already near freezing (Fig. 3a). If the entire water column is simply cooled to the freezing point, the vertical density difference is made even stronger (Fig. 3c, red crosses compared to bold black 'plus' symbols), such that a halving of the modern surface-to-deep salinity difference in the wintertime Antarctic would be required to completely counteract its effect (Fig. 3c, green crosses and dashed line). Changes in polar stratification through this mechanism would not develop until the entire ocean water column had changed temperature. Thus, this response would not be evident in model

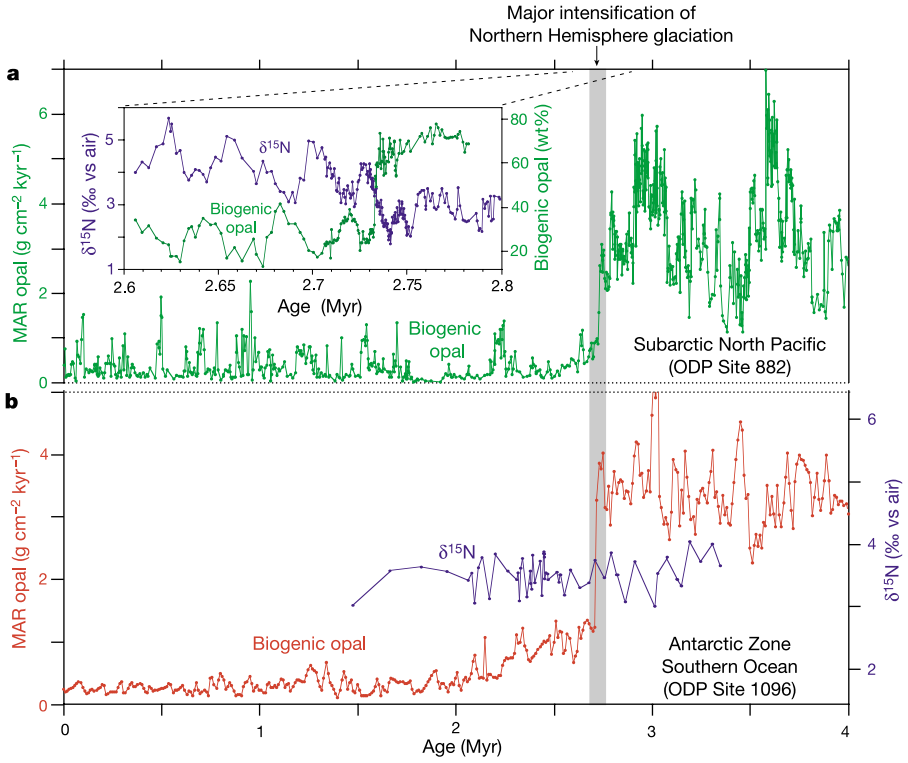

Figure 2 Subarctic North Pacific (ODP Site 882) and Southern Ocean (ODP Site 1096)[8] palaeoceanographic time series. Shown are biogenic opal accumulation over the past 4 Myr and sediment $^{15}N/^{14}N$ across the late Pliocene opal transition. **a**, Mass accumulation rate (MAR) of biogenic opal in the Subarctic North Pacific (green) decreases at the onset of major Northern Hemisphere glaciation at 2.7 Myr (more specifically, 2.73 Myr; ref. 7). Inset, fluctuations in biogenic opal percentage (green) and $\delta^{15}N$ (blue) during the time interval 2.6–2.73 Myr reveal a cycle consistent with the Milankovitch obliquity frequency (high sediment $\delta^{15}N$ correlates with abundance peaks in ice-rafted debris[7] (data not shown); $\delta^{15}N = ((^{15}N/^{14}N)_{sample}/(^{15}N/^{14}N)_{reference} - 1) \times 1{,}000‰$). **b**, Mass accumulation rate of biogenic opal in the Antarctic zone of the Southern Ocean (ODP Site 1096, red)[8] shows a decrease that is similar in structure and timing to that observed in the Subarctic North Pacific. Sediment $\delta^{15}N$ (blue) across the opal accumulation transition shows no systematic or significant change, varying between 3 and 4‰.

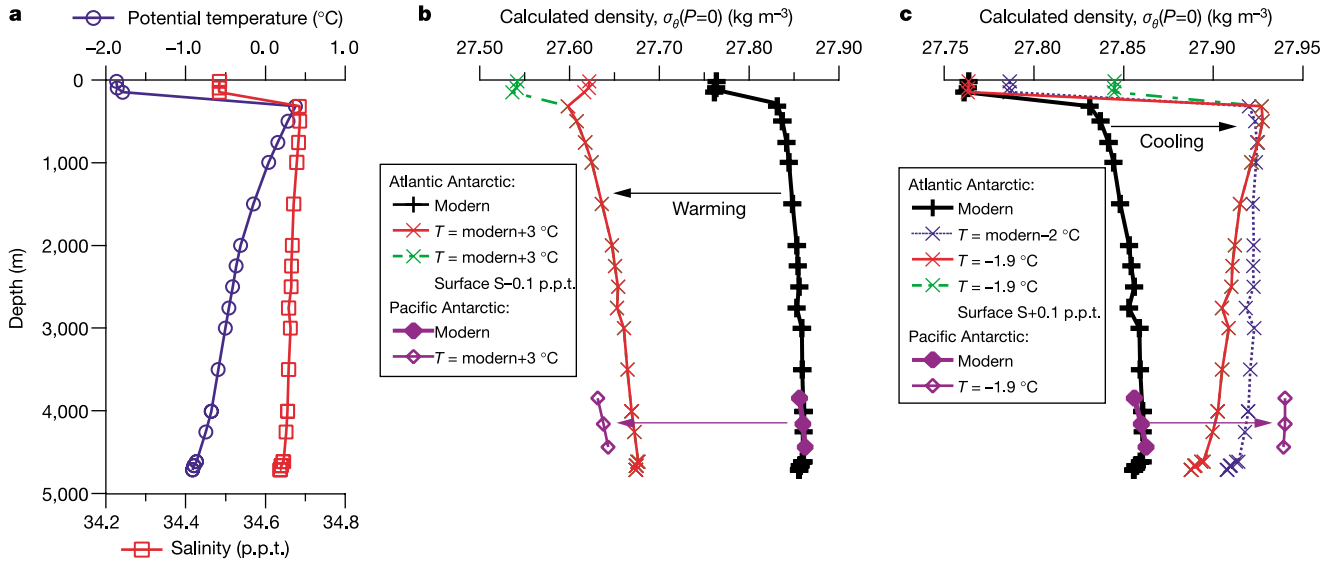

Figure 3 Density as a function of depth in the modern wintertime Antarctic and changes in this density structure for uniform changes in seawater temperature. Potential temperature (**a**, open blue circles), salinity (**a**, open red squares), and calculated potential density (**b** and **c**, bold black 'plus' symbols) for a wintertime profile in the Antarctic (WOCE SR04 station 163, Atlantic sector, 65.7° S, 38.8° W, 23 September 1989), and recalculation of potential density after several simple hypothetical changes in water column temperature and salinity (**b** and **c**, crosses). Wintertime data are used because overturning is most likely during that season, and this region is among the least vertically stable in the open Antarctic. The recalculated potential density profiles are for: (1) warming the entire water column by 3 °C (**b**, red crosses and solid line); (2) warming the entire water column by 3 °C and decreasing the salinity of the surface mixed layer by 0.1 p.p.t. (**b**, green crosses and dot-dashed line); (3) cooling the entire water column by 2 °C (**c**, blue crosses and dotted line; this would cool the shallowest and deepest waters past the freezing point); (4) cooling the entire water column to near the freezing point, −1.9 °C (**c**, red crosses and solid line); and (5) cooling the entire water column to −1.9 °C and increasing the salinity of the surface mixed layer by 0.1 p.p.t. (**c**, green crosses and dot-dashed line). Density and recalculated density after warming (**b**) and cooling (**c**) are also plotted for deep waters in the Pacific sector of the Antarctic near ODP Site 1096 (purple diamonds, filled and open, respectively; WOCE S04P station 702, 67° S, 87° W, 28 February 1992), which are warmer and saltier than deep waters in the Atlantic sector of the Antarctic.

experiments that are run for less than the ventilation time of the deep ocean[22].

One important caveat to our proposal is that, as the low latitudes cool, the atmosphere may transport less fresh water to the polar ocean, which could work to reduce the polar salinity gradient (Fig. 3, green crosses). Moreover, other physical mechanisms for a link between cooling and stratification cannot be ruled out. The westerly winds could shift equatorward and/or weaken as climate cools, leading to a decrease in wind-driven upwelling in the Antarctic[23]. The sea ice cycle redistributes fresh water within the polar regions, determining where sinking and stratification occurs in the modern polar ocean, and there is evidence for the production, during the last ice age, of extremely salty bottom water in the Antarctic owing to the formation of sea ice[2], the melting of which may have stratified the open Antarctic. However, it remains unclear whether these other mechanisms could explain the stratification of both the Antarctic and Subarctic North Pacific at 2.7 Myr.

If a polar region migrates towards stratification, positive feedbacks reinforce this change. An increase in polar ocean stratification would increase the residence time of water in the polar surface by decreasing exchange with the subsurface, allowing the surface to accumulate the fresh water being deposited from the atmosphere and thus causing further stratification. As a result, while gradual ocean cooling would motivate a gradual shift towards stratification, the positive feedback associated with freshwater accumulation may cause the onset of stratification to be abrupt, as is observed for the 2.7-Myr transition.

A positive feedback of greater global significance may operate through atmospheric carbon dioxide. The export of organic carbon out of the low-latitude surface ocean works to sequester carbon dioxide in the ocean interior, while the exposure of deep water at the polar ocean surface allows this carbon dioxide to escape back to the atmosphere if not all of the major nutrients are consumed there. The slower the ocean is ventilated at a high-nutrient polar surface region, the more the low-latitude 'biological pump' is able to drive the accumulation of surface-extracted carbon dioxide in the ocean interior[24]. By preventing the polar release of deeply sequestered carbon dioxide, stratification in both the Antarctic and the Subarctic Pacific may have amplified the climate cooling associated with the onset of Northern Hemisphere glaciation, while overturning of the polar ocean may have played a role in the poorly understood warmings of the late Oligocene and middle Miocene (see Supplementary Information). □

Methods

Ocean Drilling Program Sites 882 and 1096 are in the northwest Subarctic Pacific (50° 21′ N, 167° 35′ E; water depth 3,244 m) and eastern Pacific sector of the Antarctic (67° 34′ S, 76° 58′ W, water depth 3,152 m), respectively. Methods for the opal mass accumulation records of ODP Sites 882 and 1096 are described in refs 7 and 8, respectively, while the biogenic opal percentage record for ODP Site 882 in the inset of Fig. 2 was determined by alkaline extraction of silica[25], with replication indicating a reproducibility of ±3%.

Nitrogen isotope ratios were determined on freeze-dried and homogenized samples by on-line combustion using a ThermoQuest NC2500 elemental analyser coupled to a ThermoFinnigan DeltaPlus mass spectrometer via a ThermoFinnigan Conflo III at the University of British Columbia, Vancouver. Analytical precision is ±0.3‰ (1σ), and the values are reported relative to air N_2.

The astronomically calibrated stratigraphy for ODP Site 882 is based on magnetostratigraphy and fine tuning of GRAPE density oscillations in the orbital precession band to the summer insolation at 65° N (ref. 7). The age model for ODP Site 1096 is based on magnetostratigraphy[8]. At ODP Site 1096, the sharpest decrease in biogenic opal percentage occurs roughly 12 m below the Matuyama/Gauss magnetic reversal at 2.58 Myr, suggesting that the bulk accumulation rate change is at roughly 2.7 Myr, consistent with the established significance of 2.73 Myr for climate and sediment records in general. Accordingly, a subtle change has been applied to the original age model.

Received 4 June 2003; accepted 19 January 2004; doi:10.1038/nature02357.

1. Winton, M. The effect of cold climate upon North Atlantic Deep Water formation in a simple ocean-atmosphere model. *J. Clim.* **10**, 37–51 (1997).

2. Adkins, J. F., McIntyre, K. & Schrag, D. P. The salinity, temperature, and $\delta^{18}O$ of the glacial deep ocean. *Science* **298,** 1769–1773 (2002).
3. Mitchell, B. G., Brody, E. A., Holm-Hansen, O., McClain, C. & Bishop, J. Light limitation of phytoplankton biomass and macronutrient utilization in the Southern Ocean. *Limnol. Oceanogr.* **36,** 1662–1677 (1991).
4. Martin, J. H. & Gordon, R. M. Northeast Pacific iron distributions in relation to phytoplankton productivity. *Deep-Sea Res.* **35,** 177–196 (1988).
5. Conkright, M. E. *et al. World Ocean Atlas 2001: Objective Analyses, Data Statistics, and Figures, CD-ROM Documentation* (National Oceanographic Data Center, Silver Spring, 2002).
6. Warren, B. Why is no deep water formed in the North Pacific? *J. Mar. Res.* **41,** 327–347 (1983).
7. Haug, G. H., Sigman, D. M., Tiedemann, R., Pedersen, T. F. & Sarnthein, M. Onset of permanent stratification in the subarctic Pacific Ocean. *Nature* **40,** 779–782 (1999).
8. Hillenbrand, C.-D. & Fütterer, D. K. Neogene to Quaternary deposition of opal on the continental rise west of the Antarctic Peninsula, ODP Leg 178, Sites 1095, 1096 and 1101. *Proc. ODP Sci. Res.* **178,** 1–33 (2001).
9. Barker, P. F. & Kennett, J. P. Weddell Sea paleoceanography: Preliminary results of ODP Leg 113. *Palaeogeogr. Palaeoclimatol. Palaeoecol.* **67,** 75–102 (1988).
10. Altabet, M. A. & Francois, R. Sedimentary nitrogen isotopic ratio as a recorder for surface ocean nitrate utilization. *Glob. Biogeochem. Cycles* **8,** 103–116 (1994).
11. Andreev, A., Kusakabe, M., Honda, M., Murata, A. & Saito, C. Vertical fluxes of nutrients and carbon through the halocline in the western subarctic gyre calculated by mass balance. *Deep-sea Res. II* **49,** 5577–5593 (2002).
12. Narita, H. *et al.* Biogenic opal indicating less productive northwestern North Pacific during the glacial ages. *Geophys. Res. Lett.* **29,** doi:10.1029/2001GL014320 (2002).
13. Sigman, D. M., Altabet, M. A., Francois, R., McCorkle, D. C. & Fischer, G. The $\delta^{15}N$ of nitrate in the Southern Ocean: Consumption of nitrate in surface waters. *Glob. Biogeochem. Cycles* **13,** 1149–1166 (1999).
14. Sigmon, D. E., Nelson, D. M. & Brzezinski, M. A. The Si cycle in the Pacific sector of the Southern Ocean: seasonal diatom production in the surface layer and export to the deep sea. *Deep-sea Res. II* **49,** 1747–1763 (2002).
15. Brzezinski, M. A. *et al.* A switch from $Si(OH)_4$ to NO_3^- depletion in the glacial Southern Ocean. *Geophys. Res. Lett.* **29,** doi:10.1029/2001GL014349 (2002).
16. Lefevre, N. & Watson, A. J. Modeling the geochemical cycle of iron in the oceans and its impact on atmospheric CO_2 concentrations. *Glob. Biogeochem. Cycles* **13,** 727–736 (1999).
17. Francois, R. F. *et al.* Water column stratification in the Southern Ocean contributed to the lowering of glacial atmospheric CO_2. *Nature* **389,** 929–935 (1997).
18. Gildor, H. & Tziperman, E. Physical mechanisms behind biogeochemical glacial-interglacial CO_2 variations. *Geophys. Res. Lett.* **28,** 2421–2424 (2001).
19. Boyle, E. A. & Keigwin, L. D. Deep circulation of the North Atlantic for the last 200,000 years: geochemical evidence. *Science* **218,** 784–787 (1982).
20. Manabe, S. & Stouffer, R. J. Simulation of abrupt climate change induced by freshwater input to the North Atlantic Ocean. *Nature* **378,** 165–167 (1995).
21. Wang, Z. M., Mysak, L. A. & McManus, J. F. Response of the thermohaline circulation to cold climates. *Paleoceanography* **17,** doi:10.1029/2000PA000587 (2002).
22. Sarmiento, J. L., Hughes, T. M. C., Stouffer, R. J. & Manabe, S. Response of the ocean carbon cycle to anthropogenic climate warming. *Nature* **393,** 245–249 (1998).
23. Toggweiler, J. R. Russell, J. Shifted westerlies caused low CO_2 during cold glacial periods. *Eos* **84** (Ocean Sci. Meet. Suppl.), OS21N-06 (2003).
24. Sarmiento, J. L. & Toggweiler, J. R. A new model for the role of the oceans in determining atmospheric pCO_2. *Nature* **308,** 621–624 (1984).
25. Froelich, P. N. *et al.* Biogenic opal and carbonate accumulation rates in the Subantarctic South Atlantic: The Late Neogene of Meteor Rise Site 704. *Proc. ODP Sci. Res.* **114,** 515–532 (1991).
26. Orsi, A. H., Whitworth, T. III & Nowlin, W. D. Jr On the meridional extent and fronts of the Antarctic Circumpolar Current. *Deep-Sea Res. I* **42,** 641–673 (1995).
27. Rea, D. K., Basov, I. A., Janecek, T. R. & Palmer-Julson, A. Introduction to Leg 145: North Pacific Transect. *Proc. ODP Init. Rep.* **145,** 5–7 (1993).
28. Burckle, L. H., Gersonde, R. & Abrams, N. Late Pliocene-Pleistocene paleoclimate in the Jane Basin region: ODP Site 697. *Proc. ODP Sci. Res.* **113,** 803–809 (1987).
29. Brewster, N. A. Cenozoic biogenic silica sedimentation in the Antarctic Ocean. *Geol. Soc. Am. Bull.* **91,** 337–347 (1980).
30. Diekmann, B., Fälker, M. & Kuhn, G. Environmental history of the south-eastern South Atlantic since the middle Miocene: Evidence from the sedimentological records of ODP Sites 1088 and 1092. *Sedimentology* **50,** 511–529 (2003).

Supplementary Information accompanies the paper on **www.nature.com/nature**.

Acknowledgements This work was supported by the US NSF, Schweizer Nationalfonds, Deutsche Forschungsgemeinschaft, and by British Petroleum and Ford Motor Company through the Carbon Mitigation Initiative at Princeton University. This research used samples provided by the ODP. The ODP is sponsored by NSF and participating countries under the management of Joint Oceanographic Institutions. We thank T. F. Pedersen and K. Gordon for isotope analyses, M. Soon for analytical assistance, and C.-D. Hillenbrand for providing data from ODP Site 1096. J. D. Hays focused our attention on M. Winton's work on the climate implications of the nonlinear dependence of density on temperature. D. P. Schrag encouraged its pursuit as a general mechanism, and J. F. Adkins contributed the thoughts about the role of sea ice formation on the Antarctic shelf.

Competing interests statement The authors declare that they have no competing financial interests.

Correspondence and requests for materials should be addressed to D.S. (sigman@princeton.edu).

Hybrid fracture and the transition from extension fracture to shear fracture

Jonathan M. Ramsey* & Frederick M. Chester

Center for Tectonophysics, Department of Geology and Geophysics, Texas A&M University, College Station, Texas 77843-3115, USA

* Present address: Anadarko Petroleum Corporation, 1201 Lake Robbins Drive, The Woodlands, Texas 77380, USA

Fracture is a fundamental mechanism of material failure. Two basic types of brittle fractures are commonly observed in rock deformation experiments—extension (opening mode) fractures and shear fractures[1,2]. For nearly half a century it has been hypothesized that extension and shear fractures represent end-members of a continuous spectrum of brittle fracture types[3–6]. However, observations of transitional fractures that display both opening and shear modes (hybrids) in naturally deformed rock have often remained ambiguous, and a clear demonstration of hybrid fracture formation has not been provided by experiments[4]. Here we present the results of triaxial extension experiments on Carrara marble that show a continuous transition from extension fracture to shear fracture with an increase in compressive stress. Hybrid fractures form under mixed tensile and compressive stress states at acute angles to the maximum principal compressive stress. Fracture angles are greater than those observed for extension fractures and less than those observed for shear fractures. Fracture surfaces also display a progressive change from an extension to shear fracture morphology.

In the laboratory, a shear fracture is produced under a compressive stress state, shows displacement parallel to the failure surface, and forms at a 20°–40° angle to the maximum principal compressive stress direction, σ_1 (Fig. 1). An extension fracture forms under a tensile stress condition, displays an opening-mode displacement normal to the fracture surface, and propagates in an orientation parallel to the maximum and perpendicular to the minimum principal compressive stresses. Additional fracture types described in laboratory samples, such as wedging and longitudinal splitting during uniaxial compression, are often assumed to be forms of extension and shear fractures[1,2,7,8].

Within the compressive stress regime, the empirical Coulomb–Mohr failure criterion successfully predicts the brittle failure strength and orientation of shear fractures, at least to first order[9,10]. As implied by Mohr's hypothesis, the orientation of the fracture surface is inclined to σ_1 at a fracture angle, θ, equal to $\pi/4 - \phi/2$ or $-\pi/4 + \phi/2$, where $\tan\phi$ is the slope of the failure envelope in Mohr space[9]. The failure envelope is commonly depicted as a continuous function that crosses the transition from a compressive to a tensile stress state, and thus includes uniaxial tensile failure[11,12] (Fig. 1).

A theoretical basis for continuity across stress states is provided by the Griffith theory of fracture; the theory that forms the basis of modern linear elastic fracture mechanics[1,2]. Griffith theory captures the essential physical processes of crack propagation, and provides an energy-based failure criterion for uniaxial tensile failure. From this theory Griffith derived a criterion for brittle failure under biaxial stress states, assuming a local tensile stress condition for crack propagation[13]. Further modifications treat failure under compression where crack closure and friction are important, and are generalized to treat failure under triaxial stress[14–16]. The Griffith and modified-Griffith criteria predict a parabolic failure envelope for mixed tensile and compressive stress conditions that includes uniaxial tensile failure. The Griffith criteria have also been